

Assessment of thermo-hydraulic properties of rock samples near Takhini Hot Springs, Yukon

H. Langevin* and J. Raymond
Institut national de la recherche scientifique, Québec

T. Fraser
Yukon Geological Survey

Langevin, H., Fraser, T. and Raymond J., 2020. Assessment of thermo-hydraulic properties of rock samples near Takhini Hot Springs, Yukon. In: Yukon Exploration and Geology 2019, K.E. MacFarlane (ed.), Yukon Geological Survey, p. 57–73.

Abstract

The Takhini Hot Springs area north of Whitehorse, Yukon overlies a geothermal heat source that manifests as a 46°C water seep at surface. Despite its long-term use as a tourist swimming facility, the origins and geological setting of the hot spring remains poorly understood. The objective of this study is to assess the thermo-hydraulic properties of rock samples from drill core and outcrops near Takhini Hot Springs to better explain the presence of this hydrothermal system. A moderate rock thermal conductivity (average of $\sim 3 \text{ W m}^{-1} \text{ K}^{-1}$) and a low matrix hydraulic conductivity for consolidated rocks (on the order of 10^{-9} m s^{-1}) corresponding to a linear geothermal gradient of 16°C km^{-1} in the upper part of the Takhini well indicate conductive heat transfer between 50 and 450 m depth. Hydraulic conductivity of fractured and brecciated rocks on the order of 10^{-5} m s^{-1} , and topographic contrasts affecting the hydrostatic pressure driving groundwater flow in the area suggest that forced convective heat transfer in the bottom of the Takhini well is responsible for the strong geothermal gradient of $250^\circ\text{C km}^{-1}$ observed between 450 and 500 m depth. Steep faults appear to be a key pathway for deep groundwater to seep to surface and can explain the geothermal context in the vicinity of the Takhini well. Such a framework is a typical geothermal play type in orogenic belts. This research, therefore, helps to characterize the subsurface and provides critical information needed for a successful exploration of geothermal energy resources.

* hubert.langevin@ete.inrs.ca

Introduction

As part of the Yukon government's initiative to find green energy solutions, the Yukon Geological Survey (YGS) is researching geothermal energy potential in the territory. Despite minimal subsurface temperature data, there is evidence for potential geothermal resources in Yukon due to its proximity to the Pacific Ring of Fire, the presence of hot springs and seeps, as well as the existence of major crustal-scale structures such as the Tintina and Denali faults (Fig. 1). Regional studies conducted by the YGS, including Curie Point mapping (Witter et al., 2018) and heat potential studies from radioactive granitoid rocks (Colpron, 2019), show potential for geothermal resources. Together, these studies indicate that the southern part of Yukon is expected to have the highest geothermal heat potential in the territory, however, subsurface temperature data to validate this interpretation are sparse.

The YGS initiated their geothermal research program in 2016 using funding from both the Yukon and Canadian governments. Two temperature gradient (TG) wells were drilled in 2017 and 2018: the first near Takhini Hot Springs in south-central Yukon, and the second in the Tintina fault zone near Ross River (Fraser et al., 2019; Fig. 1). The present study provides baseline thermo-hydraulic characterization of rock units in the Takhini well and from proximal outcrops in order to understand heat transfer mechanisms controlling the geothermal resource in the region. This study includes lithology, thermal conductivity, fracture spacing and hydraulic conductivity of the rocks, as well as a regional assessment of groundwater flow, with the objective of providing a conceptual hydrothermal model. Provision of such baseline data can help understand the geological controls on the geothermal system and can reduce future exploration risk in the territory.

Background

YGS' Geothermal Research Program

The Government of Yukon (YG) is committed to reducing greenhouse gas emissions from transportation, heating, electricity generation and waste with a target of a 30% reduction in GHG emissions by 2030 (Government of

Yukon, 2019). Further, over the next 10 years, YG is committed to ensuring Yukoners have access to reliable, affordable and renewable energy. Geothermal energy fits into this climate change strategy, however, it is a resource yet to be delineated in Yukon. In 2016, the YGS initiated a geothermal research program which, to date, includes a number of technical studies (e.g., Colpron, 2019; Witter et al., 2018; Fraser et al., 2019) and a community outreach engagement program. As part of this initiative, the YGS drilled two 500 m TG wells to evaluate the geothermal gradient in specific geological settings. The first well, which is the focus of this paper, was drilled in the Takhini River valley, northwest of the city of Whitehorse, ~2 km from hot springs having a surface water outflow measuring 46°C (Fig. 1). This area is proximal to a granitoid intrusion having an average potential radiogenic heat production value of $4.1 \mu\text{W m}^{-3}$ (Colpron, 2019), which is a greater than an average granitoid ($2.5 \mu\text{W m}^{-3}$; Rybach, 1981; Hasterok and Webb, 2017; Artemieva et al., 2017). The second well is located ~15 km from the village of Ross River, in central Yukon, in a crustal-scale strike-slip fault zone known as the Tintina fault (Fig. 1). Drilling program details and TG results are summarized in Fraser et al. (2018), and highlights from the Takhini well are provided herein.

Stabilized downhole temperature was measured at intervals of 50 m in the Takhini well, with finer resolution in the uppermost part of the well. A variable geothermal gradient was found, with the upper 450 m of the well measuring 16°C km^{-1} and the bottom 50 m measuring $250^\circ\text{C km}^{-1}$ (Fig. 2; Fraser et al., 2018). This increase in temperature at the base of the well has been interpreted variably as warm groundwater flow along a fault plane or permeable layer, or an impermeable zone of conductive heat transfer from a deeper aquifer (Fraser et al., 2018). Further drilling is required to determine the thickness and extent of this area of elevated temperature gradient.

Regional geology

The Whitehorse trough is an elongated northwest-trending Early to Middle Jurassic sedimentary basin that extends 650 km from northern British Columbia to central Yukon (Fig. 1; Colpron et al., 2015). Sediments here record synorogenic marine to fluvial sedimentary

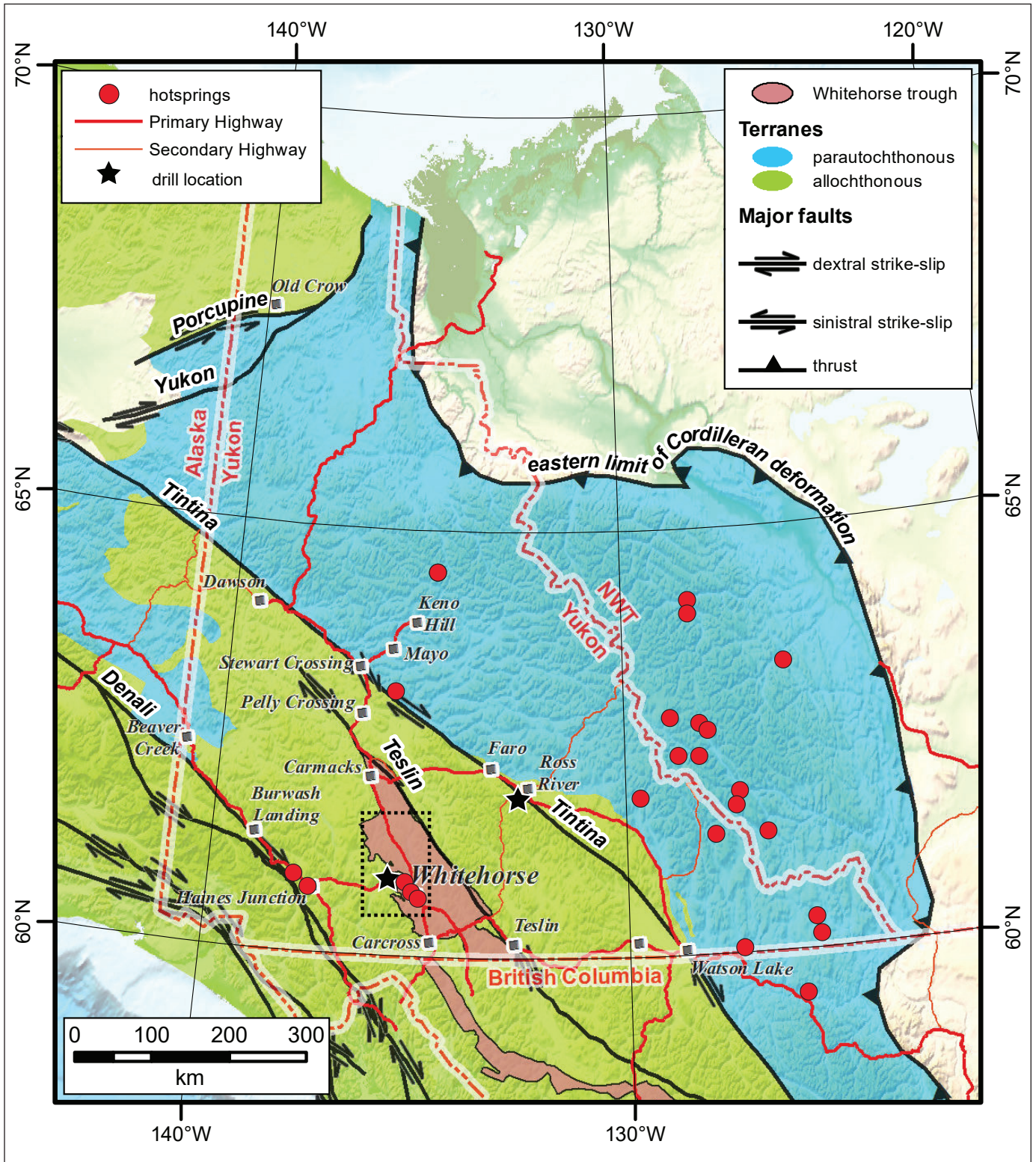


Figure 1. Terrane map of Yukon illustrating locations of major faults, hot springs, and the Whitehorse trough (orange polygon). Box indicates location of Figure 5.

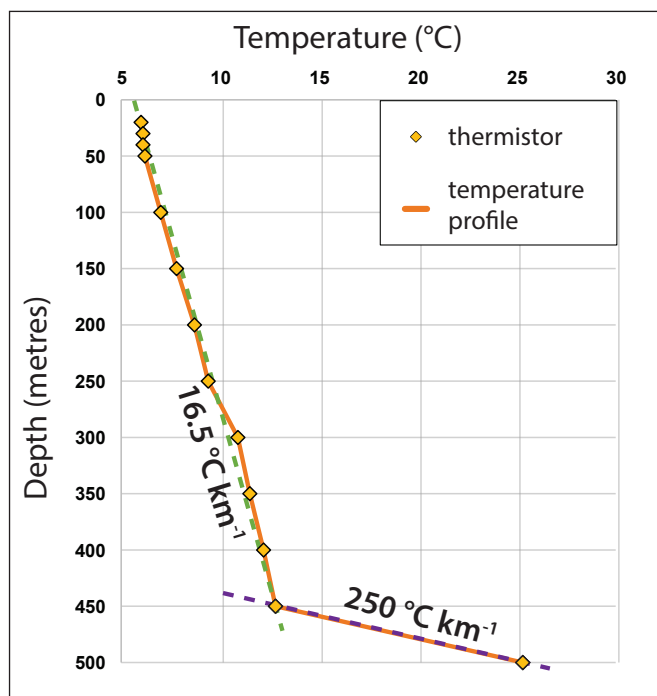


Figure 2. Downhole temperature data in the Takhini well (after Fraser et al., 2018).

and volcanic rocks in a forearc basin overlying parts of the Stikinia, Quesnellia and Cache Creek parautochthonous terranes. In the vicinity of the Takhini drill site locality, Whitehorse trough rocks include Laberge Group marine siliciclastic strata (Richtofen formation) and volcanic and volcanoclastic rocks (Nordenskiöld formation), which unconformably overlie Upper Triassic Lewes River Group siliciclastic (Casca and Mandanna members), and carbonate stratigraphy (Fig.3; Hancock member; Hart, 1997). Middle Jurassic to Paleogene granitoid plutons intruded Whitehorse trough and older strata, including an Eocene (54 Ma; Hart, 1997; Fig. 4) granitoid pluton ~2 km west of the drill site.

Methods

Core logging and field sampling

Logging of the Takhini core was undertaken at the YGS' Bostock Core Library in Whitehorse where the core is in storage. From this core, 38 thin sections were made

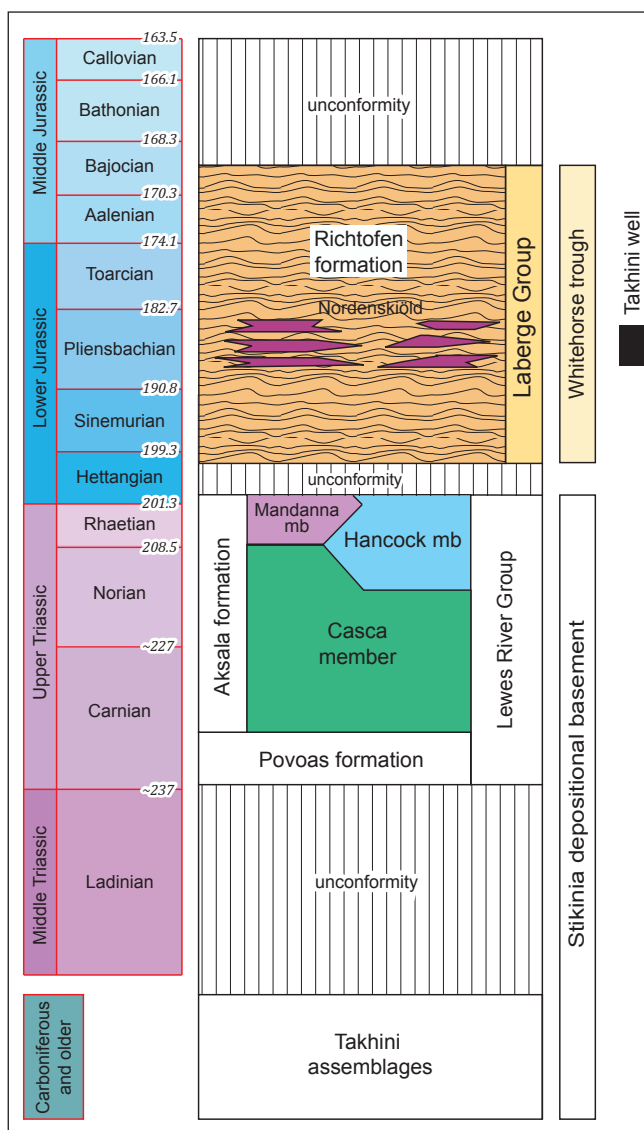


Figure 3. Sedimentary units of the Takhini well area (modified from Colpron et al., 2015). Note that Mesozoic–Cenozoic intrusive rocks are not shown.

to help define lithology and to create lithology logs. Rock outcrops found in the vicinity of the Takhini well (Fig. 4) were visited to get a better sense of stratigraphic relationships and variability in lithology to improve the number of samples for the thermo-hydraulic property analysis, and to compile geological cross sections through the well to help to define a conceptual hydrothermal system model.



Figure 4. Sampling of the Flat Creek pluton ~2 km west from the Takhini well.

Thermal conductivity

Thermal conductivity measures the amount of energy required to transfer a unit of heat through a unit distance of solid material (SI unit $\text{W m}^{-1} \text{K}^{-1}$). This property affects the geothermal gradient when conduction is the dominant heat transfer mechanism. Forty-three well samples were analyzed for thermal conductivity on one of two instruments at the Laboratoire ouvert de géothermie (LOG) at INRS, Québec City, depending upon the nature of the rock. The instruments include: (a) a Lippmann and Rauhen thermal conductivity scanner (TCS, 2017; Popov et al., 1999) used at ambient temperature for 41 consolidated rock samples; and (b) a K2D Pro needle probe from Decagon Devices Inc. (Decagon Devices Inc., 2012) used at ambient temperature for 2 unconsolidated rock samples. Thermal conductivity values are reported as ranges ± 2 standard deviations of the lithological unit averages. The units with a single sample have a range of $\pm 10\%$ considering the relative error of the measurement and the small number of samples.

Hydraulic conductivity

Hydraulic conductivity measures the ability of a fluid to move through a material's pores or fractures (SI unit in m s^{-1}). For this study, three different methods to evaluate hydraulic conductivity were used to account for variability in the mechanical properties of different rock types including consolidated, unconsolidated/brecciated and fractured rocks.

Consolidated rocks

For consolidated rocks, air permeability (measured in milliDarcies or mD) of core plugs was evaluated using a transient gas permeameter (PPP-250; Core Lab Instruments, 2016) at the LOG. This instrument forces compressed air through 4 cm diameter and 8 cm long cores, and measures the pressure decay as the air infiltrates the rock. Recorded pressures are then plotted as a function of time to calculate air permeability. Permeability values are converted to hydraulic conductivity using a factor $1 \text{ mD} = 9.6 \times 10^{-9} \text{ m s}^{-1}$ (Duggal and Soni, 1996), assuming water density and viscosity at ambient temperature. The PPP-250 was used to analyze 19 cores from the well and 16 outcrop samples. The instrument has a permeability measurement range of 0.01 to 5000 mD (9.6×10^{-11} to $4.8 \times 10^{-5} \text{ m s}^{-1}$) under ideal operating conditions. However, measurements in the range of 1 to 2 mD (9.6×10^{-9} to $1.9 \times 10^{-8} \text{ m s}^{-1}$) were assigned a value of $<1 \text{ mD}$ ($<9.6 \times 10^{-9} \text{ m s}^{-1}$) due to difficulties in keeping rock surfaces pressurized. The hydraulic conductivity values for plugs analyzed by the PPP-250 are related to primary porosity, or porosity that existed when the rock was originally formed.

Unconsolidated rocks

Two unconsolidated rock samples were evaluated for hydraulic conductivity from a major breccia/fault zone in the well at a depth of 345 m. Hydraulic conductivity (K) was evaluated from the grain size distribution of the rock fragments (Alvarado Blohm et al., 2016) using the following empirical equation (Beyer, 1966):

$$K = \frac{g \cdot 6 \times 10^{-4} \cdot \log\left(\frac{500}{d_{60}/d_{10}}\right)}{\nu} \cdot d_{10}^2 \quad (1)$$

where g is the gravitational acceleration (m s^{-2}); ν is the kinematic viscosity of water ($10^{-6} \text{ m}^2 \text{ s}^{-1}$); d_{10} is the

diameter of the 10% passing particle size (mm); and d_{60} is the diameter of the 60% passing particle size (mm). The method assumes that the hydraulic conductivity of unconsolidated rocks is related to grain size distribution affecting pore connections, where smaller grains can fill voids in between larger grains. The hydraulic conductivity reported using this method represents a bulk value for the unconsolidated rocks that have been brecciated.

Fractured rocks

Natural open fractures provide preferential paths for groundwater flow. Fracture aperture and spacing can be used to calculate hydraulic conductivity associated with secondary porosity using the Cubic Law (Witherspoon et al., 1979):

$$K = \frac{\rho \cdot g \cdot b^3 \cdot N}{12 \mu} \quad (2)$$

where ρ is the density of the rock matrix (kg m^{-3}); g is the gravitational acceleration (m s^{-2}); b is the width of the fracture (m); N is the total number of fractures per unit metre (m^{-1}); and μ is the dynamic viscosity of water ($10^{-3} \text{ kg s}^{-1} \text{ m}^{-1}$).

This method requires a manual count of natural fractures per unit distance (N) on cores and an estimation of fracture aperture (b). With this method, care must be taken not to count fractures that have occurred during or post drilling. For the Takhini core, each open fracture having mineral deposits (e.g., calcite, pyrite or chlorite precipitate) was assumed to be natural. Fracture aperture was not measured in core, as the measurements would not reflect the *in situ* conditions. Instead, aperture was assigned a constant value for the entire wellbore and the equation run for three aperture types: superfine, fine, or moderate-large. For this study, superfine was assigned apertures of 0.2 to 4 μm ; fine assigned apertures of 4 to 100 μm ; and moderate to large assigned a range of 100 to 3000 μm , based on studies by Witherspoon et al. (1979). Hydraulic conductivity values therefore are reported as ranges for each aperture type, with number of fractures per unit distance (N), which is the only variable in the equation. Further, this method assumes that fractures are interconnected and groundwater is flowing in every fracture observed.

Geological cross sections

Two cross sections were developed through the wellbore to help understand groundwater flow and heat transfer in the Takhini area.

Cross sections were made using data from existing geological maps (Yukon Geological Survey, 2018a,b), core from the Takhini well, and select outcrop samples. The extent of the cross sections was determined by the position of strategic water bodies such as the Takhini River, Takhini Hot Springs, Lake Laberge and Kusawa Lake as they represent flow boundaries (Fig. 5). Thermo-hydraulic properties measured from samples in the well and from outcrops were used to define potential regional ranges of values. All data were interpreted to define a conceptual hydrothermal model of the region.

Results

Takhini well lithology

The Takhini well is collared in volcanic and volcanoclastic rocks of the Jurassic (Pliensbachian) Nordenskiöld facies which occurs at varying stratigraphic levels within the Richthofen formation (Fig. 3). At the drill site, surface samples consist of medium to thickly bedded, poorly sorted, medium to coarse-grained sandstone having angular to subrounded grains consisting primarily of anhedral quartz and plagioclase, with up to 20% hornblende and minor chlorite. Surface bed orientation is $\sim 162^\circ/75^\circ$ SW. In the vertical wellbore, bedding dips vary from 45 to 85° from horizontal.

The top 55 m of the well were drilled using a reverse circulation drill rig and therefore no core exists from this interval. The well can be divided into 6 main lithostratigraphic units—A to F (Fig. 6). Unit A (55.0–82.9 m depth) consists of volcanoclastic sandstone and basaltic tuff, which has been intruded by mafic dikes (gabbroic–monzodioritic) between 67.5 and 77.4 m depth. Volcanoclastic sandstone (Fig. 7a) has a distinctive green color, is mainly coarse grained, locally containing pebbles and granules, poorly sorted, and is either disorganized or massive in structure, although in areas some crude reverse grading is observed. Clasts are mainly subangular to subround and dominated by mafic volcanic grains, quartz and plagioclase. Tuff is

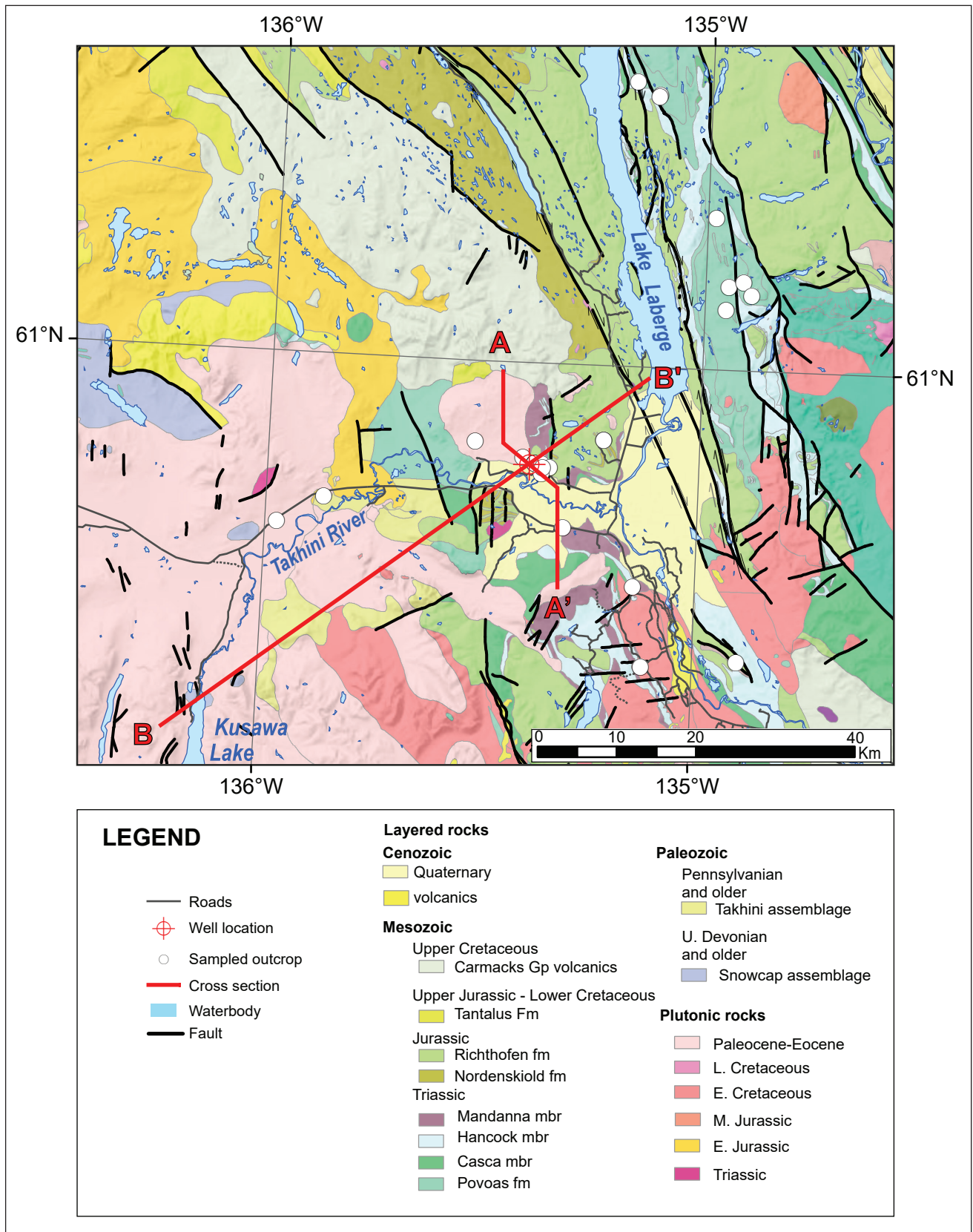


Figure 5. Geology map in the vicinity of the Takhini well, and location of cross sections shown in Fig. 9. Geology from Yukon Geological Survey (2019a).

olive green with black phenocrysts (carbonate and chlorite-replaced amphibole; Fig. 7f). Mafic dikes are dark grey with up to 25% black phenocrysts (altered plagioclase and hornblende).

Unit B (82.9–167.1 m) consists of medium and coarse volcaniclastic sandstone and minor shale. Sandstone is medium to olive-grey in color, poorly sorted, and similar in lithology to those of Unit A. Sandstone grain sizes range from fine to very coarse with coarse dominant, and shapes range from angular to subround. Pebbles and granules are rare in this unit. Crude normal grading can be observed as well as massive bedding. Shale occurs in an interval between 114.6 and 120.0 m and is black in colour, variably fractured, and cross cut by veins of calcite. The base of the unit is defined by a 10.8 m unit of highly deformed sandstone and mudstone, which shows evidence of synsedimentary deformation including load and flame structures and rip-up clasts.

Unit C (167.1–258.1 m) is a coarser grained version of Unit B that contains zones of pervasive carbonate alteration. Non-altered zones comprise mainly medium to coarse sandstone and pebbly sandstone that are medium grey to bluish grey in color. Clasts are mafic volcanic, quartz and plagioclase. Normal grading is observed in some intervals, while others have no apparent sedimentary structures. Carbonate altered zones are distinctively ‘bleached’ in appearance (Fig. 7b), are pale grey/green or grey/orange in color, and are either highly fractured or prominently cross cut with pale yellowish orange calcite veins. Carbonate is observed as matrix cement within these altered intervals.

Unit D (258.1–347.0 m) is a bluish-grey medium to very coarse volcaniclastic sandstone, variably granular, and lesser fine sandstone, siltstone and shale that is interspersed with brecciated fault zones. Sandstones

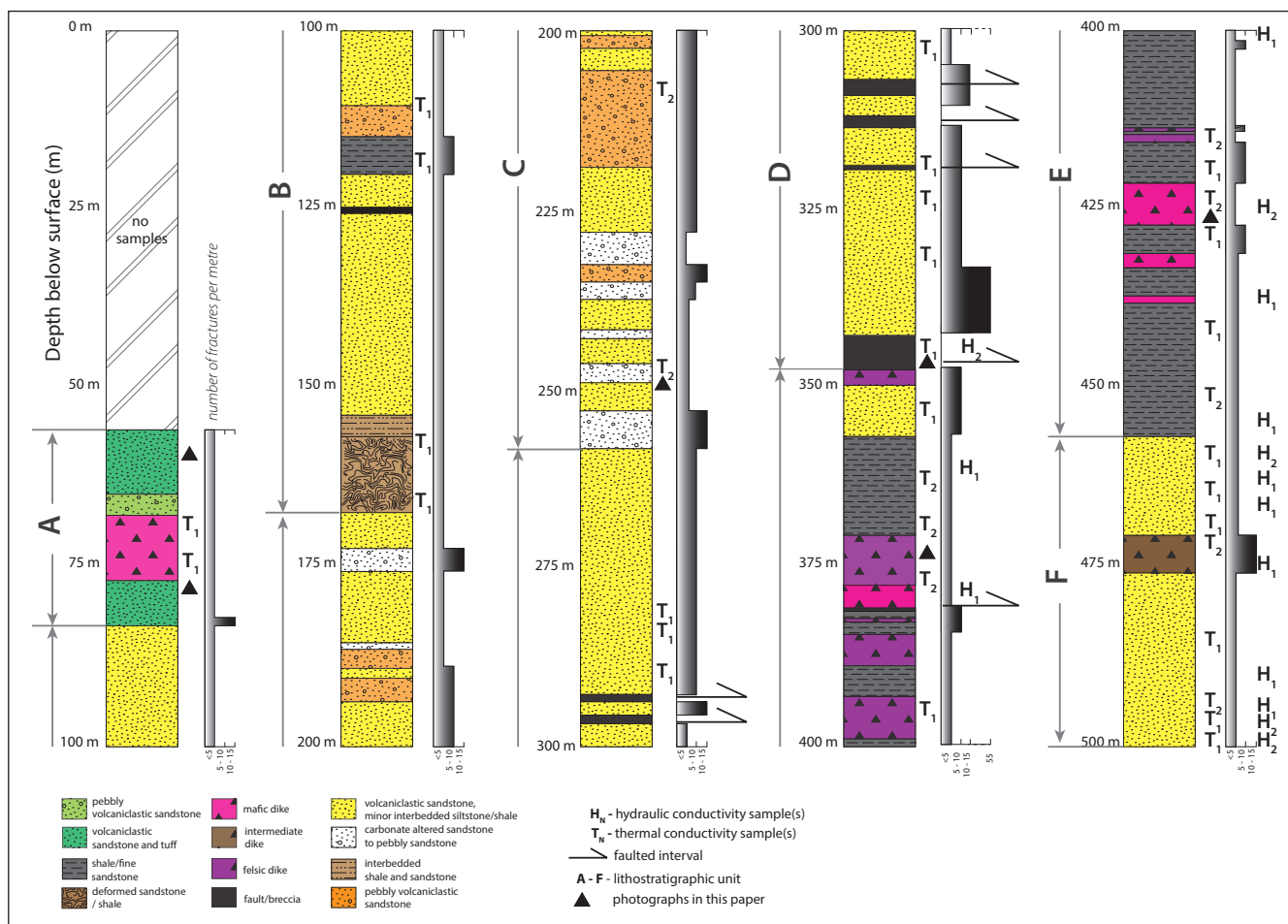


Figure 6. Lithostratigraphy of the Takhini well including fracture density, and locations of samples for thermal and hydraulic conductivity measurements.

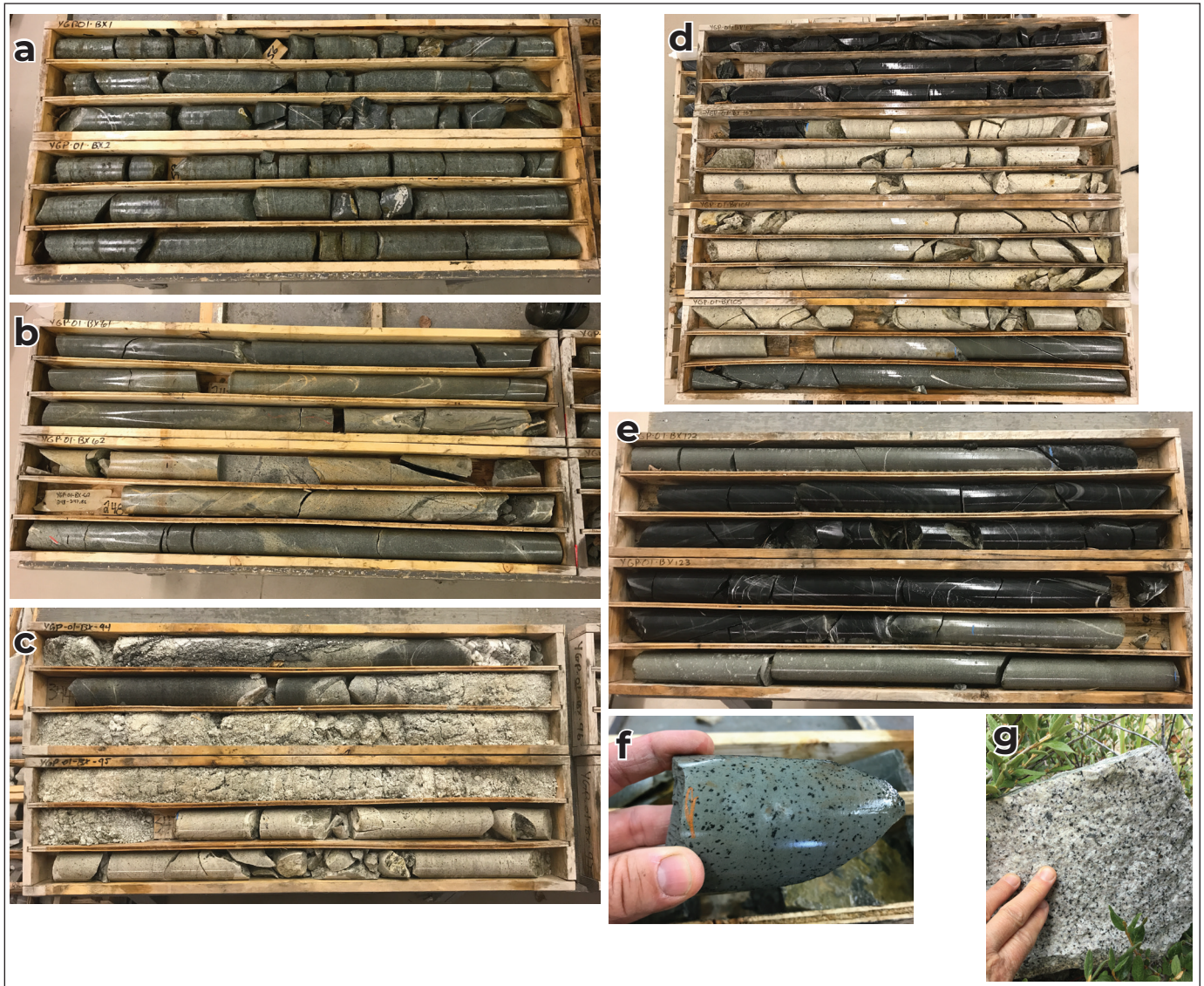


Figure 7. (a) Volcaniclastic sandstone section from top of Unit A; depth shown 55.5–62.0 m. (b) Volcaniclastic pebbly sandstone (medium to dark grey) and carbonate altered volcaniclastic pebbly sandstone (light grey and Unit C depth (~243.5–250.1 m). (c) Fault zone at the base of Unit D depth (~343.0 – 348.8 m depth). (d) Shale host rock (dark rock in top box) cut by felsic dike (light colored rock) and a mafic dike (dark colored rock at base of Box 105) in Unit E. Depth interval shown ~366.5–379.0 m. (e) Shale host rock (dark rock in box) cut by mafic dikes (lighter colored rocks at top and bottom of boxes shown) in Unit E. Depth interval shown 426.5–433.2 m. (f) Basaltic tuff observed at 82.5 m depth in Unit A. (g) Granite outcrop from ~1.5 km NW of the Takhini well. This granite forms part of the Flat Creek pluton which is part of the Nisling Range plutonic suite.

are poorly to moderately sorted, and comprise angular to subrounded altered quartz, plagioclase and mafic volcanic grains. Normally graded beds are pervasive in this unit. A thick (4.6 m) fault gouge interval defines the base of this unit (Fig. 7c), which comprises very soft and non-cohesive granular coarse sandstone containing considerable carbonate (in veins, where more cohesive, and in matrix).

Unit E (347.0–462.5 m) is a shale unit containing lesser interbedded siltstone and sandstone, which is cut by a series of mafic and felsic dikes. Felsic dikes occur above 414.1 m, are very light grey to yellowish-grey in color with black phenocrysts (Fig. 7d), and are granitic and fine-grained, with quartz and plagioclase minerals dominant, occurring as either phenocrysts or spherules. Plagioclase is often altered to carbonate. Minor minerals include white mica and scant cubic pyrite. Mafic dikes

are light bluish grey in color, gabbroic to monzogabbroic and occur more commonly below 421 m depth (Fig. 7e). These dikes are fine-grained, plagioclase-rich (in part altered to epidote) with minor hornblende (variably altered to chlorite) and biotite and up to 10% opaque minerals.













Unit F (462.5–500.0 m) is predominantly a coarse volcanoclastic sandstone succession and lesser fine sandstone and siltstone, which is cut by an intermediate dike. Sandstone is medium grey in color, and consists of poorly sorted angular to subangular quartz and plagioclase grains and minor plagioclase feldspar, mica, carbonate and chlorite. The core surface has a distinctive mottled appearance. Sedimentary structures can be observed where sandstone is interlaminated with silt and shale, as well as crude normal grading in some sandstone beds with scoured bed bases. An intermediate (borderline diorite/monzodiorite/

monzogabbro) dike cross cuts the sandstone between 470.3 and 475.8 m. The dike comprises fine-grained plagioclase lathes and minor phenocrysts, as well as carbonate and mica, and rare opaque minerals. (Fig.6).

Thermal conductivity

Thermal conductivity averages and ranges for each lithology type in the Takhini well are reported in Table 1, and complete data sets are in Appendix A. Note that there is no data for the ‘pebbly volcanoclastic sandstone’ and ‘volcanoclastic sandstone and mafic tuff’ units (green units in Fig. 6), as the rock properties were deemed similar to the volcanoclastic sandstone, minor interbedded siltstone and shale unit (yellow unit in Fig. 6) of which 14 samples were taken. Thermal conductivity values in the well range from 0.63 to 4.19 W m⁻¹ K⁻¹; the highest average value is in the deformed sandstone and shale unit (3.81 W m⁻¹ K⁻¹),

Table 1. Thermal conductivity of rock formations in the Takhini well.

Lithology description	Lithology graphic	Average thermal conductivity (W m ⁻¹ K ⁻¹)	Thermal conductivity (low; high) (W m ⁻¹ K ⁻¹)	Number of samples
Deformed sandstone and shale		3.81	[3.43; 4.19]	1
Carbonate altered sandstone to pebbly sandstone		3.47	[3.05; 3.89]	3
Felsic dike		3.38	[3.18; 3.58]	5
Interbedded shale and sandstone		3.28	[2.95; 3.61]	1
Shale and fine sandstone		3.16	[2.32; 4.00]	7
Pebbly volcanoclastic sandstone		3.16	[3.02; 3.30]	3
Intermediate dike		3.06	[3.04; 3.08]	2
Volcanoclastic sandstone, minor interbedded siltstone and shale		2.94	[2.64; 3.24]	14
Mafic dike		2.39	[2.15; 2.63]	5
Fault/breccia		0.98	[0.63; 1.33]	2
Pebbly volcanoclastic sandstone		-	-	0
Volcanoclastic sandstone and mafic tuff		-	-	0

and the lowest average value is in the breccia unit ($0.98 \text{ W m}^{-1} \text{ K}^{-1}$). Generally, average values are between 3.0 and $4.0 \text{ W m}^{-1} \text{ K}^{-1}$, except for the mafic dike and the fault/breccia units, which have values $\leq 2.4 \text{ W m}^{-1} \text{ K}^{-1}$.

Hydraulic conductivity

Consolidated and unconsolidated rocks

Table 2 includes average hydraulic conductivity derived for consolidated and unconsolidated rocks. Figure 6 displays sample locations in the well and the comprehensive results are in Appendix B. Measurements made using the PPP-250 indicate a hydraulic conductivity generally $<9.6 \times 10^{-9} \text{ m s}^{-1}$ for consolidated rocks, and having a maximum of $1.6 \times 10^{-7} \text{ m s}^{-1}$.





















For brecciated rock samples at a depth of 345 m, hydraulic conductivity measures 8.3×10^{-4} and $2.9 \times 10^{-4} \text{ m s}^{-1}$ (Table 2), which were averaged to $5.6 \times 10^{-4} \text{ m s}^{-1}$ for comparison with results obtained from other methods.

Fractured rocks

Fracture spacing ranges from 2 to 52 fractures per metre along the well, with most values <10 (Fig. 6). Ranges of hydraulic conductivity of fractured rocks are shown in Figure 8. Overall values for the entire well are on the order of 10^{-14} – $10^{-10} \text{ m s}^{-1}$ for superfine apertures, 10^{-10} – 10^{-6} m s^{-1} for fine apertures, and 10^{-6} – 10^{-1} m s^{-1} for moderate to large apertures. For fractures having $\sim 100 \mu\text{m}$ apertures (lower part of moderate), the values are on the same order of magnitude as the unconsolidated rocks of the breccia/fault zone in the well at a depth of 345 m ($\sim 10^{-4} \text{ m s}^{-1}$; Table 2).

The highest value of hydraulic conductivity related to fracture porosity is in a well-fractured interval (52 fractures per metre) at a depth of 332–341 m in a volcanoclastic sandstone with minor siltstone and shale unit (yellow on Fig. 6). For this interval, hydraulic conductivity is: 3.4×10^{-13} to $2.8 \times 10^{-9} \text{ m s}^{-1}$ for a superfine fracture aperture (0.2–4 μm); 2.8×10^{-9} to $4.3 \times 10^{-5} \text{ m s}^{-1}$ for fine fracture aperture (4–100 μm); and 4.3×10^{-5} to $1.2 \times 10^0 \text{ m s}^{-1}$ for a moderate to large

Table 2. Hydraulic conductivity of consolidated and unconsolidated rocks in the Takhini well.

Rock Type	Lithology	Well Depth (m)	Hydraulic conductivity (m s^{-1})
Consolidated		302.83 - 303.07	$<9.6 \times 10^{-9}$
		325.16 - 325.34	$<9.6 \times 10^{-9}$
		363.17 - 363.32	$<9.6 \times 10^{-9}$
		378.89 - 379.09	$<9.6 \times 10^{-9}$
		401.86 - 402.08	$<9.6 \times 10^{-9}$
		423.03 - 423.18	$<9.6 \times 10^{-9}$
		424.58 - 424.76	1.6×10^{-7}
		439.86 - 440.00	7.4×10^{-8}
		455.00 - 455.25	$<9.6 \times 10^{-9}$
		459.27 - 459.43	$<9.6 \times 10^{-9}$
		461.44 - 461.59	$<9.6 \times 10^{-9}$
		462.85 - 463.00	$<9.6 \times 10^{-9}$
		467.00 - 467.15	$<9.6 \times 10^{-9}$
		475.00 - 475.28	$<9.6 \times 10^{-9}$
		485.95 - 486.10	$<9.6 \times 10^{-9}$
		493.10 - 493.25	$<9.6 \times 10^{-9}$
		496.40 - 496.50	$<9.6 \times 10^{-9}$
	497.00 - 497.15	$<9.6 \times 10^{-9}$	
Unconsolidated		497.84 - 498.00	$<9.6 \times 10^{-9}$
		345.32 - 345.52	2.9×10^{-4}
		346.00 - 346.20	8.3×10^{-4}

fracture aperture (100–3000 μm ; Fig.8). The lowest hydraulic conductivity related to fracture porosity occurs in the lower part of the well at a depth of 465 m in a volcanoclastic sandstone with minor siltstone and shale unit having 2.2 fractures per metre. Hydraulic conductivity calculated for a superfine fracture aperture at this depth ranges from 1.4×10^{-14} to $1.2 \times 10^{-10} \text{ m s}^{-1}$, for fine fracture apertures range from 1.2×10^{-10} to $1.8 \times 10^{-6} \text{ m s}^{-1}$ and for moderate to large fracture aperture from 1.8×10^{-6} to $4.9 \times 10^{-2} \text{ m s}^{-1}$ (Fig. 8). Results are subject to an important variability since fracture aperture is hardly measurable on core samples.

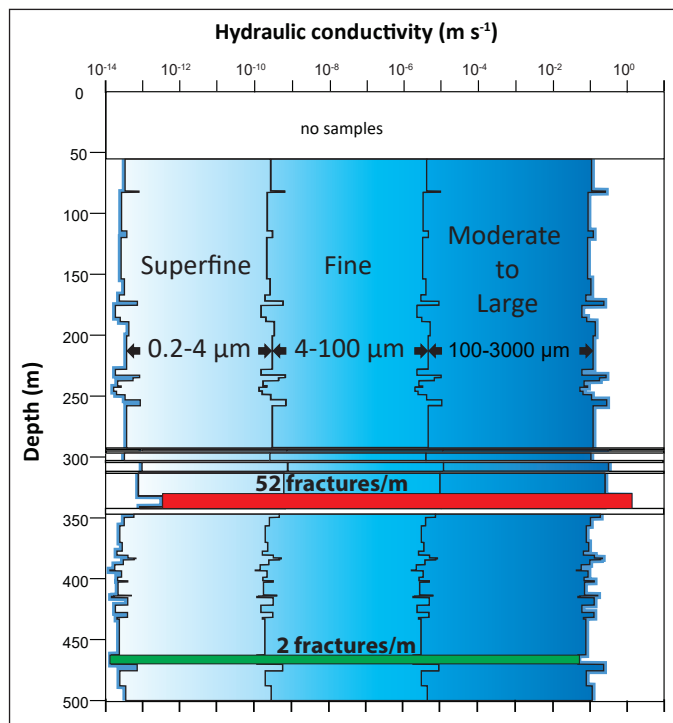


Figure 8. Hydraulic conductivity of fractured rocks in the Takhini well analyzed for superfine, fine, and moderate-to-large fracture aperture.

Geological cross sections

Interpreted cross sections A–A' and B–B' (Figs. 5 and 9a,b) show the distribution of geological units influencing heat transfer and groundwater flow in the vicinity of the Takhini well. Basement rocks consist of variably deformed and metamorphosed greenschist of the Takhini assemblage. Triassic–Jurassic sedimentary sequences and volcanoclastic strata overlie the Takhini assemblage. Steeply dipping north trending normal faults separate the sedimentary basin into segments as a result of regional tectonic activity in pre-Late Cretaceous time (Hart, 1997). Eocene granitic and granodioritic plutons intruded Triassic–Jurassic sedimentary sequences and volcanoclastic strata (Hart, 1997). Fault extensions and thickness of rock units at depth are interpretive due to the lack of geophysical or deep well data in this area.

Discussion

Geological interpretation of the Takhini well

Lithology in the Takhini well is assigned to Lower Jurassic Laberge Group sediments that have been intruded by younger plutonic rocks and subjected to faulting. Sandstones are immature and have a high concentration of poorly sorted angular to subrounded volcanic fragments, feldspar and quartz, and have crude sedimentary structures, both primary and secondary. These rocks are similar in description to sandstones interpreted as distal Laberge Group exhibiting characteristics of deposition from turbidity currents and subject to substantial post-depositional reworking based upon outcrop on the shore of Lake Laberge (Hutchison, 2017), ~30 km northwest of the Takhini site. Laberge Group sediments were deposited in a forearc basin derived from the exhumation of flanking arc terranes when orogenesis was beginning in the southern Canadian Cordillera (Pliensbachian and later; Colpron et al., 2015). The majority of the sandstone and shale in the well is currently assigned to the Richthofen formation. However, the immaturity of the sandstone and the presence of crystal tuff, particularly in the upper part of the well (55–80 m), suggests a proximal volcanic source and some of these units may be assigned to the Nordenskiöld formation. The Nordenskiöld formation is defined by a series of crystal tuff layers within the Laberge Group varying from 50–350 m thick that are Jurassic in age (Sinemurian to Pliensbachian; 190.5 ± 1.5 Ma weighted average; Colpron et al., 2015). The tuff layers comprise mainly coarse-grained (2–4 mm) euhedral feldspar, quartz, having broken corners, and fewer fine-grained (1–2 mm) hornblende and biotite crystals containing sparse lithic grains (Hart, 1997). Part of this unit may have a strong sedimentary character, which is interpreted as reworked older tuff horizons. Further studies are required to delineate the exact assignment of these rocks to either the Nordenskiöld or the Richthofen formations.

Cross cutting the Laberge Group sediments are felsic and mafic dikes most commonly observed in the lower part of the well in Unit E, but there is also an intermediate dike in Unit F, and a mafic dike in Unit A.

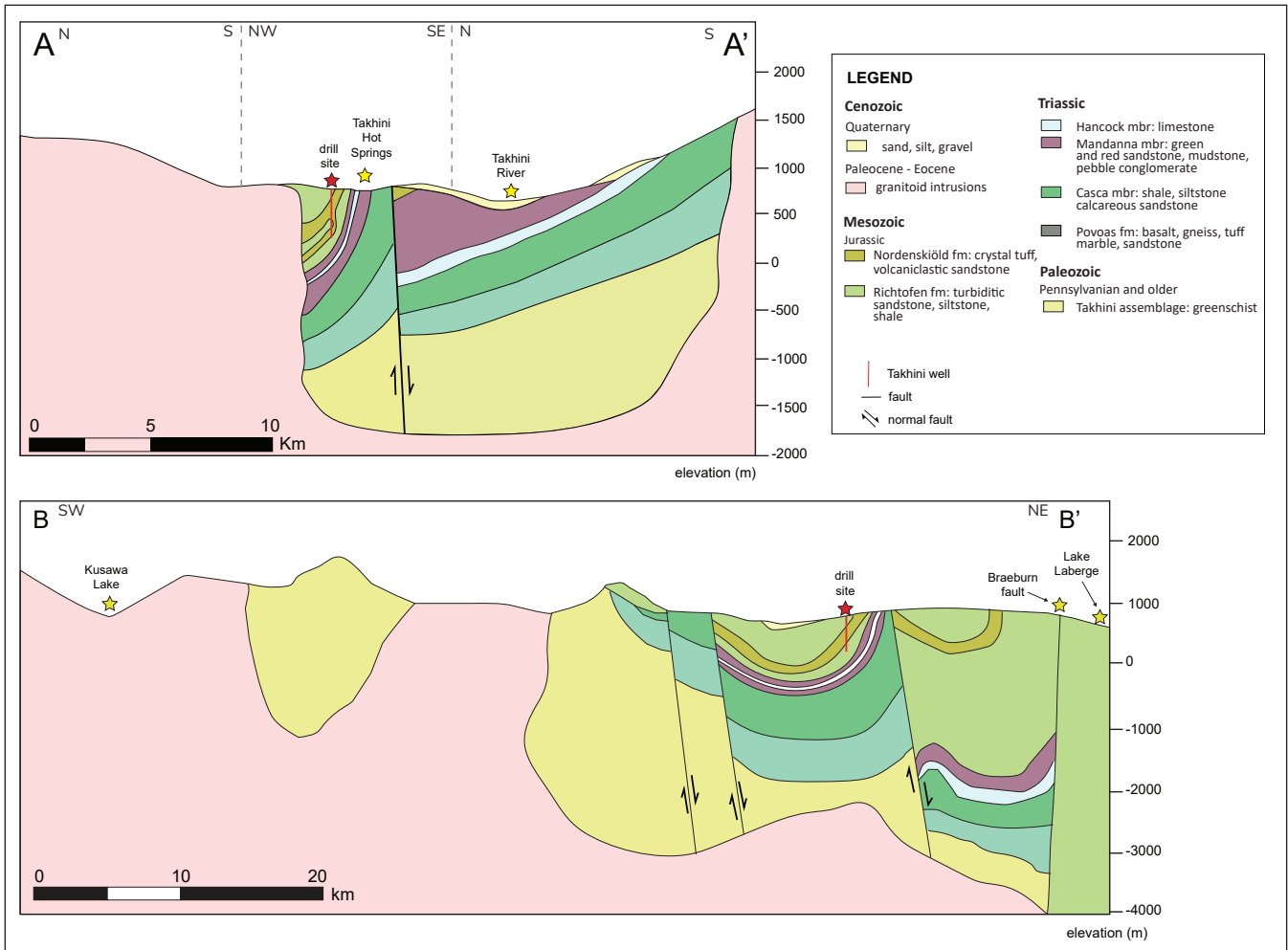


Figure 9. (a) Cross section A-A' showing the geological interpretations in the vicinity of the Takhini well. Location of cross section in Figure 5. Geology after Hart (1997) and Colpron et al. (2015). **(b)** Cross section B-B' showing the geological interpretations in the vicinity of the Takhini well. Location of cross section in Figure 5. Geology after Hart (1997) and Colpron et al. (2015).

It is unknown at this time if these intrusive rocks are coeval, or if they are related to the pluton that crops out to the west of the well (Fig. 5), which is Eocene in age (53.6 ± 0.2 Ma) and associated with older fault reactivation due to regional tectonic stress (Hart, 1997). There is evidence in the well that faulting occurred post dike emplacement. For example, there is a faulted upper contact of a felsic dike interval at a depth of 342 m. However, cross cutting relationships are not always observed, and future radiogenic dating of the rocks would provide meaningful age constraints.

Heat Transfer Mechanisms

Temperature measurements and analysis of thermo-hydraulic properties in the Takhini well indicate that

conduction and forced convection are the main heat transfer mechanisms occurring in the upper and lower parts of the well, above and below 450 m, respectively.

The faint thermal conductivity contrasts among units associated with a smooth and near-linear temperature profile above 450 m depth is characteristic of heat conduction. Thick formations of low thermal conductivity, generally $< 2 \text{ W m}^{-1} \text{ K}^{-1}$, can induce a thermal blanket effect and increase the geothermal gradient. This insulating effect is not observed in the well because there is no lithology that has such a low thermal conductivity, except for the breccia unit ($0.98 \text{ m}^{-1} \text{ K}^{-1}$) that only covers 2% of the well length.

Conductive heat transfer cannot explain the high temperature gradient of $250^{\circ}\text{C km}^{-1}$ observed below 450 m depth as thermal conductivity contrasts of the host rock are similar to the rocks above. The temperature anomaly in the lower part of the well is instead interpreted as forced-convective heat transfer due to deep groundwater rising along fractures. The assessment of hydraulic properties confirms this hypothesis. Sass and Götz (2012) suggest that transitional states of natural convective to forced convective heat transfer can occur in rocks within high (10^{-5} m s^{-1}) to low (10^{-9} m s^{-1}) hydraulic conductivity, while conductive heat transfer mostly occurs in rocks of low hydraulic conductivity ($<10^{-9} \text{ m s}^{-1}$; Fig. 10). The matrix hydraulic conductivity of rock samples in the Takhini well and surrounding outcrops commonly have values $<9.6 \times 10^{-9} \text{ m s}^{-1}$ which indicates that heat convection can only occur in fractured and unconsolidated rocks, where hydraulic conductivity was confirmed higher. Figure 10 shows that fine to large fracture apertures can be sufficient to allow different transitional states of forced convective to auto convective heat transfer. A large aperture for all fractures is, however, unlikely.

Natural or auto convection responsible for groundwater movement can only occur under significant temperature contrasts in rocks having high hydraulic conductivity (Sass and Götz, 2012). For example, this can occur in a volcanic environment, where deep groundwater flow in permeable formations is driven by fluid buoyancy due to shallow magmatic intrusions. On the other hand, forced convection implies groundwater flow driven by

hydrostatic pressure variations in an aquifer system that can be of moderate hydraulic conductivity. An example of this scenario is where topographic highs in a mountain range act as a recharge zone for water that discharges in lower altitude valleys. Groundwater flow can thus be controlled by the regional hydraulic gradient caused by topography when there is adequate fracture connectivity in the host rock. Fractures and unconsolidated rocks in the well have a hydraulic conductivity that is at least greater than 10^{-9} m s^{-1} . This can lead to forced convective heat transfer and trigger the formation of a hydrothermal system giving rise to hot springs, provided that fractures are interconnected. The Takhini well and the hot spring are located in a trough having important topographic contrasts (Fig. 9a,b), where the difference in elevation ($\sim 500 \text{ m}$ over $\sim 15 \text{ km}$ distance) can cause such a strong hydraulic gradient. However, the Takhini well represents a relatively small window to assess hydraulic properties and does not provide sufficient information to evaluate fracture connectivity. Consequently, it is difficult to correlate any permeable zones observed in the core samples of the Takhini well with the high geothermal gradient at the bottom of this well ($>450 \text{ m}$). The forced convective heat transfer hypothesis remains the most plausible. Assuming that faults and fractures are interconnected, regional groundwater flow can be directed toward the Takhini River and upflow can occur along faults, creating resurgence under the Takhini well near the river, a major waterbody collecting groundwater.

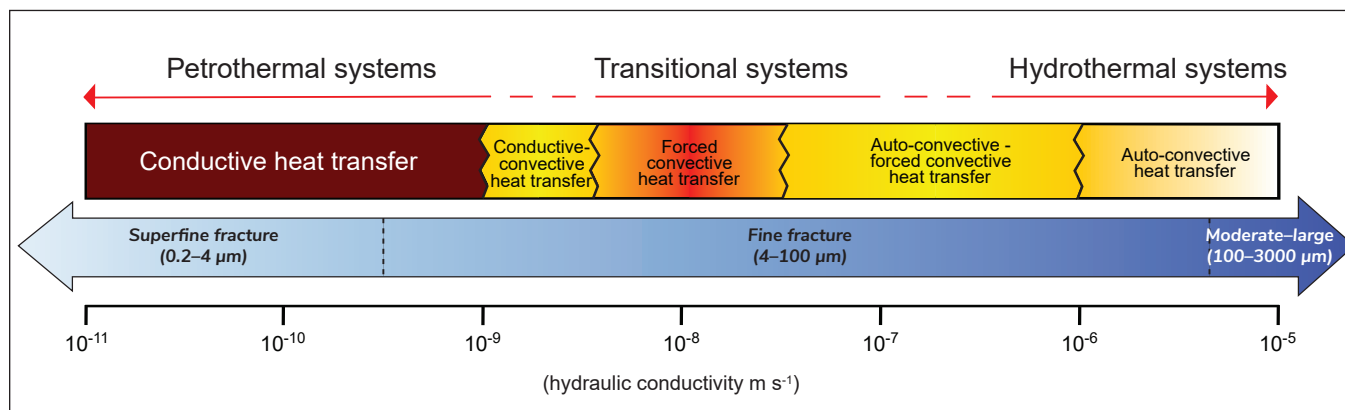


Figure 10. Generalized characterization of geothermal systems based on major mechanism of heat transfer (convective vs conductive; after Sass and Götz, 2012).

Conceptual Hydrothermal Model

The geological setting in the Takhini area is typical of an orogenic belt, where conductive and forced convective heat transfer can occur (Moeck et al. 2014). Geological features, such as steeply dipping crustal faults, can favour forced convective heat transfer as they are preferential paths for rising warm groundwater. Figure 11 shows schematic isotherms and water flow line interpretations based on the main recharge areas and major faults. The primary groundwater recharge areas are associated with elevated mountainous regions and the discharge dominantly occurs near the Takhini River. From recharge to discharge, groundwater tends to flow through permeable rocks. Several north-trending steep normal faults cut strata in the Takhini area (Hart, 1997). One of these faults is at the center of the hydrothermal model. This major feature can affect the groundwater flow path as it is believed to be more fractured and permeable than rocks outside the fractured zone. Due to the hydraulic head difference between the top and the base of the fracture, deep water can rise along the fault to create shallower isotherms. This can

form hot springs like Takhini Hot Springs where well-connected fractures allow a constant groundwater discharge.

Conclusions

This study has defined the thermo-hydraulic properties of rocks in, and within, the vicinity of the Takhini temperature gradient well in southern Yukon. These data are co-interpreted with the measured temperature gradient at this well and offers explanations for mechanisms of heat transfer in the subsurface. In addition, a conceptual hydrothermal model of the Takhini area is presented. The thermal conductivity results show that conductive heat transfer dominates the well to a depth of 450 m, as the temperature profile is near-linear and thermal conductivity contrasts are faint. The elevated geothermal gradient observed at the bottom of the Takhini well ($250^{\circ}\text{C km}^{-1}$) and the thermal manifestations at Takhini Hot Springs are likely caused by forced convective heat transfer associated with deep groundwater flow in permeable fractures generating a hydrothermal system typical of a geothermal play type in an orogenic belt (Fig. 11).

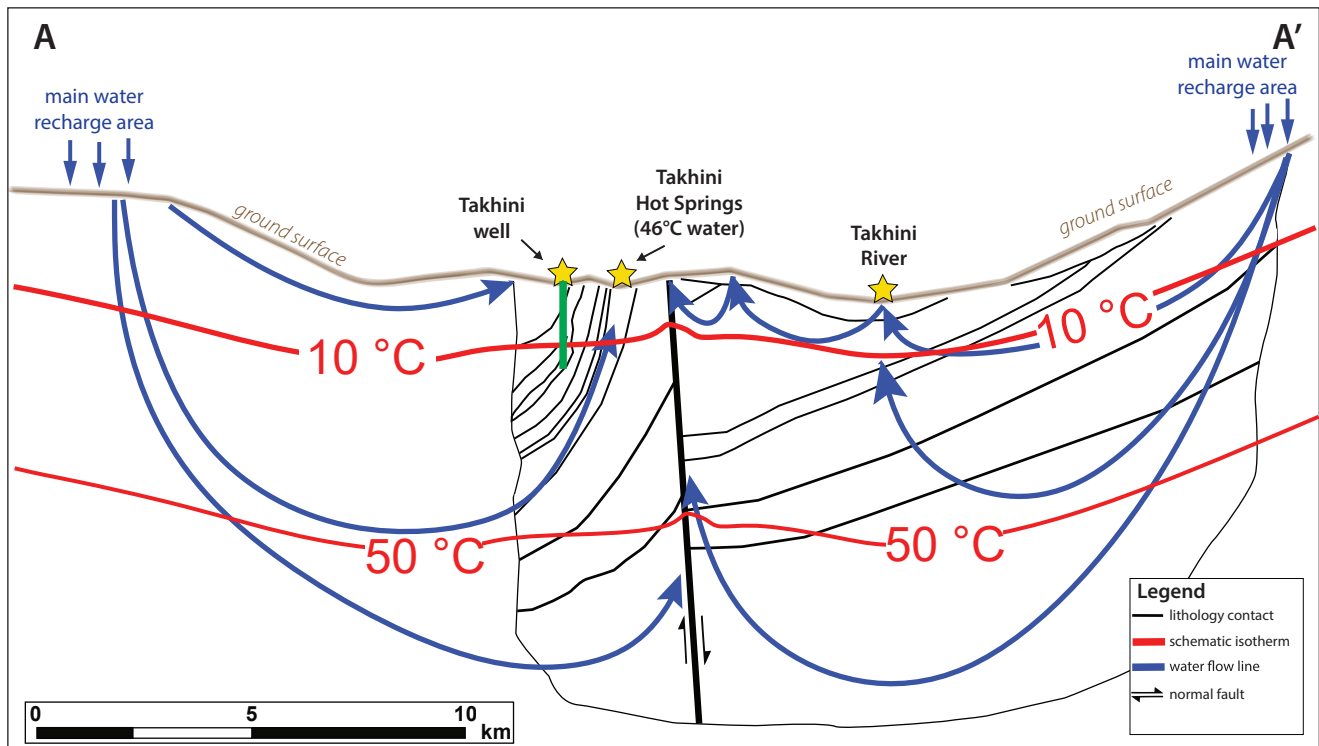


Figure 11. Interpreted hydrothermal system of the Takhini Hot Springs area according to geothermal play types in orogenic belts; after Moeck, (2014).

The ~2 km lateral distance between warm water at the bottom of the Takhini well and the Takhini Hot Springs can give an idea about the potential extent of this warm fluid reservoir, assuming there is interconnectivity of fractures between those sources. However, further work is needed to assess the extension and the interconnectivity of those water sources.

Assessment of the thermal conductivity can be used with additional calculated radiogenic heat values from intrusive bodies in the region as a next step to evaluate heat flow and extrapolate temperature at depth. Quantifying the natural amount of heat originating from the Earth interior and based on Fourier's Law, the heat flux density is needed to define boundary conditions of numerical groundwater flow and heat transfer models to quantitatively confirm the heat transfer hypotheses formulated in this work. Such an approach would be helpful to improve understanding of the origin of the Takhini Hot Springs. These models can be used to reproduce the temperature measured in the Takhini well or at the hot spring to better explain the factors controlling the formation of the hydrothermal system.

The Yukon geological context shows potential for geothermal energy with many hot springs like Takhini. Geothermal exploration done by the YGS provides more data to evaluate this potential around the hot springs. Further calculation and simulations with the measurements obtained with this study will bring a better comprehension of resources to move towards the exploitation of geothermal energy in this region.

Acknowledgements

The Takhini well was drilled on Category A land of the Ta'an Kwäch'än Council. We are grateful for the opportunity to work with this Yukon First Nation, and for access to their land in summer 2019 to evaluate outcrops. This work was funded by a Discovery grant from the Natural Sciences and Engineering Research Council of Canada awarded to INRS and a scholarship from the Armand-Frappier Foundation awarded to the first author. Jeff Witter of Innovate Geothermal Inc. is acknowledged for reviewing this paper. Maurice Colpron (YGS) provided field, technical, and GIS guidance for which we are appreciative. Liam Maw is acknowledged for thin section descriptions.

References

- Alvarado Blohm F.J., Urzua, A., Ebel, J. and Kafka, A., 2016. Determination of hydraulic conductivities through grain-size analysis. MSc thesis, Boston College University Libraries, Chestnut Hill, United States, p. 102.
- Artemieva, I.M., Thybo, H., Jakobsen, K., Sørensen, N.K. and Nielsen, L.S.K., 2017. Heat production in granitic rocks: Global analysis based on a new data compilation GRANITE2017. *Earth Science Reviews*, vol. 172, p. 1–26.
- Beyer, W. 1966. Hydrogeological investigations in the deposition of water pollutants. *Journal of Applied Geology*, vol. 12, p. 599–606.
- Colpron, M., Crowley, J.L., Gehrels, G.E., Long, D.G.F., Murphy, D.C., Beranek, L.P. and Bickerton, L., 2015. Birth of the northern Cordilleran orogen, as recorded by detrital zircons in Jurassic synorogenic strata and regional exhumation in Yukon. *Lithosphere*, vol. 7, p. 541–562.
- Colpron, M., 2019. Potential radiogenic heat production from granitoid plutons in Yukon. Yukon Geological Survey, Open File 2019-16, 1 map and data.
- Core Lab Instruments, 2016. PPP-250 Portable probe permeameter operations manual. Core Lab Instruments. Tulsa, United States, p. 6.
- Decagon Devices Inc., 2012. KD2 Pro Thermal properties analyser: operator's manual, version 12. Decagon Devices Inc., Pullman, United States, p. 68.
- Duggal, K.N. and Soni, J.P., 1996. *Elements of Water Resources Engineering*. New Age International (P) Limited, p. 270.
- Fraser, T.A., Grasby, S.E., Witter, J.B., Colpron, M. and Relf, C., 2018. Geothermal studies in Yukon—collaborative efforts to understand ground temperature in Canadian North. *GRC Transactions*, vol. 42, 20 p.
- Fraser, T., Colpron, M. and Relf, C., 2019. Evaluating geothermal potential in Yukon through temperature gradient drilling. In: *Yukon Exploration and Geology 2018*, K.E. MacFarlane (ed.), Yukon Geological Survey, p. 75–90.

- Hart, C.J.R., 1997. A transect across northern Stikinia: Geology of the northern Whitehorse map area, southern Yukon Territory (105D/13-16). Yukon Geological Survey, Bulletin 8, p. 112.
- Hasterok, D. and Webb, J., 2017. On the radiogenic heat production of igneous rocks. *Geoscience Frontiers*, vol. 8, <https://doi.org/10.1016/j.gsf.2017.03.006>
- Hutchison, M.P., 2017. Whitehorse trough: Past, present and future petroleum research – with a focus on reservoir characterization of the northern Laberge Group. Yukon Geological Survey, Open File 2017-2, 48 p. plus appendices and plates.
- Moeck, I.S., 2014. Catalog of geothermal play types based on geologic controls. *Renewable and Suitable Energy Reviews*, vol. 37, p. 867–882. <https://doi.org/10.1016/j.rser.2014.05.032>
- Popov, Y.A., Pribnow, D.F.C., Sass, J.H., Williams, C.F. and Burkhardt, H., 1999. Characterization of rock thermal conductivity by high-resolution optical scanning. *Geothermics*, vol. 28, p. 253–276.
- Rybach, L. 1981. Geothermal systems, conductive heat flow, geothermal anomalies. In: *Geothermal systems: principles and case histories*, Muffler LJP, Rybach, L. (eds), John Wiley & Sons, New York.
- Sass, I. and Götz, A.E., 2012. Geothermal reservoir characterization: a thermofacies concept. Blackwell Publishing: Terra Nova, vol. 24, p. 142–147, <https://doi.org/10.1111/j.1365-3121.2011.01048.x>.
- TCS, 2017. Thermal Conductivity (TC) and Thermal Diffusivity (TD) Scanner, manual. Lippmann and Rauen, Schaufling, Germany, p. 53.
- Witherspoon, P.A., Wang, J.S.Y., Iwai, K. and Gale, J.E., 1979. Validity of Cubic law for fluid flow in a deformable rock fracture. University of California, Berkeley, p. 28.
- Witter J.B., Miller C.A., Friend M. and Colpron, M., 2018. Curie Point Depths and Heat Production in Yukon, Canada. Proceedings of the 43rd Workshop on Geothermal Reservoir Engineering, Stanford University, Stanford, California, February 12–14, 11 p.
- Yukon Geological Survey, 2018a. Bedrock geology data set. Yukon Geological Survey, <https://data.geology.gov.yk.ca/Compilation/3>, accessed Nov. 2019.
- Yukon Geological Survey, 2018b. Surficial geology data set. Yukon Geological Survey, <https://data.geology.gov.yk.ca/Compilation/33>, accessed Nov. 2019.
- Government of Yukon, 2019. Draft of our clean future: a Yukon strategy for climate change, energy and a green economy. Government of Yukon, Whitehorse, Canada, p. 61.

Appendices

The appendices are only available as digital files. They are included in a .zip file that accompanies this document, and are available from <https://data.geology.gov.yk.ca/>.

Appendix A. (1) Thermal conductivity scanner measurements for consolidated rocks using a Lippman and Rauen thermal conductivity scanner (TCS, 2017). **(2)** Thermal conductivity needle probe measurements for unconsolidated rocks with the K2D Pro needle probe (Decagon Devices Inc., 2012).

Appendix B. (1) Hydraulic conductivity measurements for consolidated rocks using a transient gas permeameter (PPP-250; Core Lab Instruments, 2016). **(2)** Hydraulic conductivity measurements for unconsolidated rocks from the grain size distribution (Beyer, 1966).

